Title

Caveolae-associated cAMP/Ca2+-mediated mechano-chemical signal transduction in mouse atrial myocytes

Authors

Medvedev, Roman Y
Turner, Daniel GP
DeGuire, Frank C
et al.

Publication Date

2023-11-01

DOI

10.1016/j.yjmcc.2023.10.004

Peer reviewed

HHS Public Access

Author manuscript

J Mol Cell Cardiol. Author manuscript; available in PMC 2024 November 01.

Published in final edited form as:

J Mol Cell Cardiol. 2023 November ; 184: 75–87. doi:10.1016/j.yjmcc.2023.10.004.

Caveolae-associated cAMP/Ca^{2+}-mediated mechano-chemical signal transduction in mouse atrial myocytes

Roman Y. Medvedev, PhD[1], **Daniel G. P. Turner, BS**[1,#], **Frank C. DeGuire, BS**[1,#], **Vladislav Leonov, PhD**[1], **Di Lang, PhD**[1,2], **Julia Gorelik, PhD**[3], **Francisco J. Alvarado, PhD**[1], **Vladimir E. Bondarenko, PhD**[4], **Alexey V. Glukhov, PhD**[1,*]

[1] –Department of Medicine, University of Wisconsin-Madison School of Medicine and Public Health, Madison, WI, USA;

[2] –Department of Medicine, University of California San Francisco, San Francisco, CA, USA;

[3] –National Heart and Lung Institute, Imperial College London, London, United Kingdom;

[4] –Department of Mathematics and Statistics, Georgia State University, Atlanta, GA, USA.

Abstract

Caveolae are tiny invaginations in the sarcolemma that buffer extra membrane and contribute to mechanical regulation of cellular function. While the role of caveolae in membrane mechanosensation has been studied predominantly in non-cardiomyocyte cells, caveolae contribution to cardiac mechanotransduction remains elusive. Here, we studied the role of caveolae in the regulation of Ca^{2+} signaling in atrial cardiomyocytes. In Langendorff-perfused mouse hearts, atrial pressure/volume overload stretched atrial myocytes and decreased caveolae density. In isolated cells, caveolae were disrupted through hypotonic challenge that induced a temporal (<10 min) augmentation of Ca^{2+} transients and caused a rise in Ca^{2+} spark activity. Similar changes in Ca^{2+} signaling were observed after chemical (methyl-β-cyclodextrin) and genetic ablation of caveolae in cardiac-specific conditional caveolin-3 knock-out mice. Acute disruption of caveolae, both mechanical and chemical, led to the elevation of cAMP level in the cell interior, and cAMP-mediated augmentation of protein kinase A (PKA)-phosphorylated ryanodine receptors (at Ser^{2030} and Ser^{2808}). Caveolae-mediated stimulatory effects on Ca^{2+} signaling were abolished via inhibition of cAMP production by adenyl cyclase antagonists MDL12330 and SQ22536, or reduction of PKA activity by H-89. A compartmentalized mathematical model of mouse atrial myocytes linked the observed changes to a microdomain-specific decrease in phosphodiesterase activity, which disrupted cAMP signaling and augmented PKA activity. Our findings add a new dimension to cardiac mechanobiology and highlight

[*]**To whom correspondence should be addressed:** Glukhov AV, 8455 WIMR II, 1111 Highland Ave., Madison, Wisconsin 53705, USA. aglukhov@medicine.wisc.edu.

[#]These authors contributed equally

Disclosures

None declared.

caveolae-associated cAMP/PKA-mediated phosphorylation of Ca^{2+} handling proteins as a novel component of mechano-chemical feedback in atrial myocytes.

Graphical Abstract

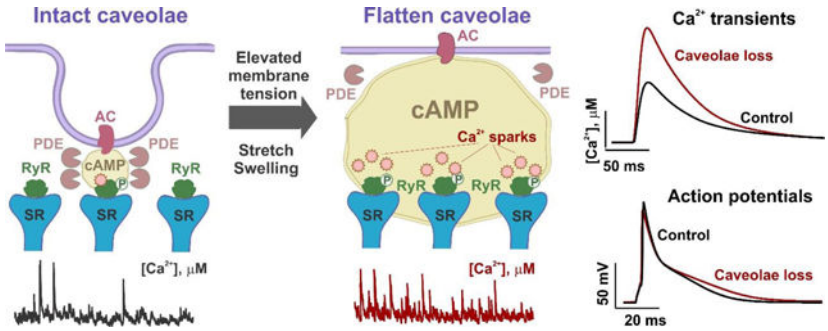

Keywords

Atrial myocyte; Stretch; Calcium dynamics; Cyclic adenosine monophosphate; Ryanodine receptor; protein kinase A; Caveola

1. Introduction

Mechanical load is one of the most important regulators of cardiac function. Cardiomyocyte membrane plasticity is required for sensing and transmitting mechanical signals. Specialized structures called caveolae help provide this plasticity [1]. Caveolae are small (50–100 nm) invaginations of the plasma membrane that are enriched with cholesterol, sphingolipids, and scaffolding proteins called caveolins. Caveolae play a major role in the adaptation to membrane tension by buffering “extra” membrane in various cell types, including cardiomyocytes. The mechanosensitive functions of caveolae could be particularly important for atrial myocytes, which have a less organized transversal tubule system than ventricular myocytes [2], and demonstrate a 2–3-fold higher expression of caveolae compared to ventricular cells [3]. It is estimated that caveolae increase the plasma membrane surface area by 27% in ventricular myocytes [4] versus 56% in atrial cells. Furthermore, compared to ventricular myocytes, atrial cells have unique Ca^{2+} signaling [5], different hemodynamics, and distinct mechanisms of arrhythmogenesis. Despite these differences, most studies of caveolae in the heart, including those focused on mechanobiology, were performed on ventricles, and the role of caveolae in mechano-mediated regulation of Ca^{2+} signaling in atrial cardiomyocytes (ACMs) remains poorly understood.

Recent studies indicate that caveolae may contribute to mechano-induced modulation of Ca^{2+} signaling via compartmentalized regulation of cyclic adenosine monophosphate (cAMP) dynamics in cardiac myocytes [6,7]. It was shown that muscle-specific caveolar scaffolding protein caveolin-3 (Cav3) concentrates various proteins within the caveolae microdomain, including G-protein coupled receptors, as well as adenylyl cyclases (ACs), and phosphodiesterases (PDEs) [8]. Downregulation of Cav3 in failing ventricular myocytes [9], expression of the dominant negative Cav3 mutant [10], or disruption of caveolae by

cholesterol depleting agent methyl-β-cyclodextrin (MβCD) [6] converts the sarcolemma-confined cAMP signal to a global cell-wide pattern that may affect phosphorylation of cytosolic proteins. Indeed, MβCD-induced caveolae disruption significantly increased the twitch amplitude and the rates of cell shortening and relaxation [11] in rat ventricular myocytes, increasing both diastolic and systolic $[Ca^{2+}]_i$ and CaT amplitude [7]. Thus, we hypothesize that caveolae contribute to mechano-induced modulation of Ca^{2+} signaling via spatial-temporal control of cAMP signaling and cAMP-mediated phosphorylation of Ca^{2+} handling proteins in ACMs.

We used an established model of atrial volume overload in Langendorff-perfused *ex vivo* mouse hearts [12] that resulted in an elevated membrane tension and caveolae downregulation. In *in vitro* experiments using isolated ACMs, caveolae were disrupted through hypotonically increased membrane tension, cholesterol depletion (via MβCD), and cardiac-specific conditional Cav3 knockout. We found that in all these condition, caveolae disruption led to augmentation of Ca^{2+} signaling that was associated with the elevation of cAMP level in the cell interior, cAMP-mediated upregulation of protein kinase A (PKA) activity, and PKA-phosphorylation of ryanodine receptors (RyRs). A novel compartmentalized mathematical modeling of mouse ACMs [13], linked the observed findings to a caveolae-specific regulation of PDEs. Our findings add a new dimension to cardiac mechanobiology and highlight caveolae-associated cAMP/PKA-mediated phosphorylation of Ca^{2+} handling proteins as a novel component of mechano-chemical feedback in ACMs.

2. Methods

For a detailed description of methods, see Expanded Methods in the Data Supplement.

2.1. Animals

Adult (3 to 5-month-old) male and female cardiac-specific Cav3 knock-out mice (Cav3KO) and wildtype littermate controls (WT) were used in the study. The male outbred, Sprague Dawley rats (*rattus norvegicus*, 200–500 g) were obtained from Charles River, USA. Cav3KO mice were generated as in [14,15] by crossing a mouse line with loxP-flanked exon 2 of Cav3 with an α-myosin heavy chain proto-oncogene tyrosine-protein kinase MER Cre recombinase proto-oncogene tyrosine-protein kinase MER (aMHC-MERCreMER) mouse. Tamoxifen was delivered in the form of tamoxifen-laced food, at 0.5 mg tamoxifen/1 g pulverized chow, reconstituted with 1 mL H_2O/1 g chow, reformed, and dried for 24–48 h. Mice remained on the diet for 14 days and euthanized 14 days post tamoxifen treatment.

2.2. In vitro atrial volume overload model

To apply graded stretch to the intact atria, a Langendorff perfusion protocol modified for murine heart was used [12]. Briefly, hearts were retrogradely perfused under constant aortic pressure (60–80 mmHg) and superfused with oxygenated Tyrode solution of the following composition (in mmol/L): 128.2 NaCl, 4.7 KCl, 1.19 NaH_2PO_4, 1.05 $MgCl_2$, 1.3 $CaCl_2$, 20.0 $NaHCO_3$, and 11.1 glucose (pH=7.35±0.05, 37°C). The caval and pulmonary veins were ligated. The interatrial septum was perforated to ensure pressure equilibration between

left and right atria. A polyimide tube (ID: 0.0249”, OD: 0.073”; Cole-Parmer) was inserted into the coronary sinus and connected to a pressure monometer (MLT844, AD Instruments) to monitor biatrial pressure. Another polyimide tube was inserted into the pulmonary artery, so perfusion fluid left the heart exclusively through this tube. Atrial pressure and degree of atrial dilatation were controlled by adjustment of the height of the pulmonary outflow tube.

2.3. Mouse ACM isolation

Mouse ACMs were enzymatically isolated as previously described [16]. Briefly, hearts were extracted, cannulated, and perfused with Tyrode’s solution (37°C) containing the following (in mmol/L): 140 NaCl, 6 KCl, 1 $MgCl_2$, 1 $CaCl_2$, 10 glucose and 10 HEPES, pH=7.4 (NaOH). Left and right atrial appendages were dissected and washed with “low Ca^{2+}/Mg^{2+}-free” solution containing the following (in mmol/L): 140 NaCl, 5.4 KCL, 1.2 KH_2PO_4, 0.066 $CaCl_2$, 50 taurine, 18.5 D-glucose, 5 HEPES and 1 mg/ml bovine serum albumin (BSA), pH=6.9 (NaOH), followed by “low Ca^{2+}/Mg^{2+}-free” solution containing 1 mg/ml collagenase from *Clostridium histolyticum* (type 2, Worthington) and 0.2 mg/ml elastase (Worthington) for 12 min (37°C). Isolated cardiomyocytes were readapted to extracellular Ca^{2+} concentration of 1.0 mmol/L. Rat ACMs were isolated using the similar protocol [3], except digestion was performed with collagenase (1 mg/ml; Worthington) and hyaluronidase (0.6 mg/ml; Sigma-Aldrich) for 20 min.

2.4. Cell swelling

To increase membrane tension and mechanically disrupt caveolae, cell swelling was induced by changing the osmolarity of cell bathing solution from isotonic Tyrode’s solution (IT, in mmol/L: 91 NaCl, 5.3 KCL, 1.2 KH_2PO_4, 0.5 $MgCL_2$, 1 $CaCl_2$, 10 glucose, 10 HEPES, with pH 7.4 and Mannitol 91 mM, 300 mOsm) to hypotonic Tyrode’s (HT, composition is same as IT, except mannitol, 210 mOsm) [17].

2.5. Scanning ion conductance microscopy (SICM)

SICM was used to visualize changes in ACM topography during stretch [3]. The analysis of cell surface z-groove organization determined as a ratio between the total lengths of z-grooves observed on the image to the estimated value from the image with an ideal z-groove structure [3].

2.6. Transmission electron microscopy (TEM)

Langendorff-perfused hearts from volume overload model and isolated ACMs were fixed in phosphate buffer with 2.5% glutaraldehyde and 2.0% paraformaldehyde for 12 hours, post-fixed in 1% osmium tetroxide, dehydrated in a graded ethanol series, rinsed in propylene oxide, and embedded in Epon 812 substitute. The samples were sliced into 70-nm sections, post-stained in 8% uranyl acetate in 50% EtOH and Reynold’s lead citrate and viewed on a Philips CM120 transmission electron microscope. TEM images were analyzed by using the Fiji software. [18,19]

2.7. Intracellular confocal Ca^{2+} recordings

Intracellular Ca^{2+} measurements were performed from freshly isolated ACMs as previously described [20]. Cells were incubated in IT with 5 μM Fluo-4 AM (Invitrogen) and 0.4% Pluronic F-127 (Invitrogen) for 25 minutes. Then, the dye was washed out and cells were kept in fresh isotonic Tyrode's solution. Experiments were performed using Leica SP5 (Ca^{2+} sparks) or LSM510 Meta confocal microscope (Carl Zeiss) at 2.35 ms/line as previously described [16]. The protocol for Ca^{2+} transients included 30 s of field pacing at 1 Hz and application of IT/HT buffer containing 1 mM of caffeine for 30 sec. Cells were paced at 1 Hz for 30 s to increase SR Ca^{2+} loading and then the local Ca^{2+} release events were recorded under 40× oil immersion objective, pinhole of 1 airy unit. The analysis of Ca^{2+} sparks was made with the SparkMaster plugin [21] in Fiji with the detection criteria set at 4.2. [22]

2.8. Isolated cardiomyocytes immunofluorescence labeling

ACMs were fixed with methanol, blocked with 2% BSA, and incubated overnight with the respective primary antibodies in blocking solution at 4°C. The total RyR2 (1:500, MA3–916, ThermoFisher Scientific) raised in mouse and one of the rabbit-raised phosphor-specific antibodies: custom-made RyR2-Ser^{2030} (1:200, provided by Dr. Alvarado [23]), RyR2-Ser^{2808} (1:200, A01031AP, Badrilla), and RyR2-Ser^{2814} (1:200, A01030AP, Badrilla). The cells were then washed and incubated with Alexa-conjugated secondary antibodies (Molecular Probes) diluted 1:800 in blocking solution. Imaging was performed with a Leica SP5 Confocal microscope under 63×/1.40 NA oil immersion objective. The colocalization percent was analyzed by BlobProb plugin in Fiji [24].

2.9. Foster resonance Energy Transfer (FRET) microscopy

Isolated rat ACMs were plated (around 5,000) on coverslips, and cultured for 48 h in M199 media with adenovirus encoding the plasma membrane-targeted EPAC (pmEPAC) or cytosolic-EPAC cAMP sensors [14]. Cell fluorescence was split into YFP (535/40 nm) and CFP (480/30 nm) channels using DualView (Optical Insights) and monitored by ORCA-ER CCD camera (Hamamatsu Photonics, UK). After baseline FRET measurements in IT, a 0.3T (to make a final 0.7T solution) or IT solutions were added to start swelling or isotonic recordings, respectively. In separate experiments, IT with MβCD was added to a final concentration of 10 mM to remove caveolae. After 15 min of measurements, 1 mM IBMX with 10 μM of Forskolin was added to the cells to inhibit PDEs and stimulate ACs, respectively, to measure the maximal cAMP level. cAMP responses were calculated in reference to this maximal cellular cAMP responses.

2.10. Mathematical models of mouse ACMs

We used a compartmentalized mathematical model of mouse ACMs recently developed by Asfaw et al. [13] with minor modifications. The only change we added to the transition rate between the states of ryanodine receptors by increasing rates k_a^+ and k_b^+ by a factor 2 and by multiplication the rates k_a^- and k_b^- by a factor 0.5 to stabilize Ca^{2+} release. The resulting modifications did not change the action potential and slightly reduced $[Ca^{2+}]_i$

transient (from 0.465 μM to 0.425 μM, 8.6% decrease), which is within the variability of the experimental data.

To investigate the effects of caveolae reduction on the mouse ACMs, we performed simulations with control model and with the models with hypothetical changes of the model parameters that could be a result of the caveolae loss. Both control and modified models were run for 10 minutes (600 s) after the caveolae loss, and time dependencies of cAMP concentration in three compartments (caveolar, extracaveolar, and cytosol) were obtained for 10-minute periods. All simulations were performed on a single processor under SUSE Linux 11 on a Dell Precision Workstation T3500 with a six-core Intel Xeon CPU W3670 (3.2 GHz, 12 GB RAM).

2.12. Statistical analysis

Data are presented as mean ± S.E.M. Student t test was used in 2-group comparisons (paired for comparisons between the same participant and unpaired for 2 groups of different participants). Multiple groups of normally distributed data of similar variance were compared by 1- or 2-way ANOVA when appropriate. For multiple comparisons, the Tukey corrected p-value is shown. All statistical analyses were performed using GraphPad Prism 8 (GraphPad Software). A value of $p<0.05$ was considered statistically significant.

3. Results

3.1. Elevated membrane tension caused caveolae disruption

To model *ex vivo* acute atrial stretch, we used atrial pressure/volume overload in Langendorff-perfused mouse hearts through an increase in end diastolic volume by elevating pulmonary artery pressure (Fig. 1A, B). This model led to a statistically significant atrial distension accompanied by an increase in myocyte width (~15%) and length (~25%; Fig. 1C) and elongation of sarcomeres in both atria (~20%, Fig. 1D). TEM analysis linked atrial distension to a significant increase in the membrane tension (as estimated through the membrane convolution index [18,19]) and reduction in caveolae density by ~60% (Fig. 1E).

To further estimate cellular changes upon mechanical disruption of caveolae in isolated ACMs, we applied a hypotonic (HT) swelling protocol [25]. HT challenge caused a significant increase in cell width (~20%, Fig. 2A), without change in cell length. SICM topographical analysis of swelled myocytes revealed a significant decrease in Z-groove index (a measure of surface regularity [3], Fig. 2B), confirming changes in cardiomyocyte topography during elevated membrane tension. Importantly, TEM analysis (Fig. 2C) showed that HT protocol decreased the membrane convolution index already at 1 min of swelling and resulted in a significant reduction of caveolae density (Fig. 2D) as observed during *ex vivo* atrial distension (Fig. 1E), and thus could be used to model stretch-induced caveolae disruption and its effects on Ca^{2+} signaling in ACMs.

3.2. Mechanical disruption of caveolae temporally augments Ca^{2+} signaling

To determine the effects of mechanically disrupted caveolae on intracellular Ca^{2+} signaling, confocal line scan imaging was performed on isolated ACMs during HT protocol applied for

16 min (Fig. 3A and B). HT swelling caused a temporal increase of Ca^{2+} transient (CaT) amplitude that significantly differed from the IT condition at the 8th min and then returned to control values after 12 min of swelling (Fig. 3C). HT protocol also caused a temporal prolongation of CaT time to peak at 1–4th min (Fig. 3D). We did not find significant changes in CaT decay time and decay rate constant during swelling. We estimated the effects of HT on sarcoplasmic reticulum (SR) Ca^{2+} loading by caffeine induced Ca^{2+} release (Fig. 3B). SR Ca^{2+} load did not change significantly during HT protocol (Fig. 3E). The rate constant for caffeine-induced CaTs, which mainly represents Ca^{2+} transport via Na^{+}/Ca^{2+}-exchanger and the plasma membrane Ca^{2+} ATPase, was found to be elevated after 1 min of HT and then reduced to IT levels after 4 min of swelling (Fig. 3F).

Stretch-induced augmentation of Ca^{2+} signaling was accompanied by elevation of spontaneous Ca^{2+} release from the SR (Fig. 3G, H). Furthermore, we found a significant increase in spontaneous Ca^{2+} spark (CaSp) activity during swelling (Fig. 3I), specifically at 1 min, which returned to IT levels at around 8th min of swelling (Fig. 3J). These findings indicate a biphasic response of ACMs to stretch characterized by a transient augmentation of Ca^{2+} signaling during first 1–8 mins of mechanical stimulation, with a subsequent reduction to baseline levels.

3.3. Disruption of caveolae recapitulates swelling-induced changes in spontaneous Ca^{2+} signaling

To confirm that caveolae disruptions augments Ca^{2+} signaling, we employed two alternative models of caveolae downregulation through (1) cholesterol depletion via 30 min incubation of ACMs with 10 mM of MβCD, and (2) genetic deletion of caveolae scaffolding protein Cav3 in Cav3KO mice. TEM analysis confirmed ~60% reduction of caveolae density in MβCD-treated cells and ~50% reduction of caveolae density in Cav3KO cells compared to wild-type myocytes (Fig. 4A, B). In both MβCD-treated and Cav3KO ACM, we found a significant increase in CaSp frequency (Fig. 4C, D), similarly to the HT-induced CaSp activity. We used a caffeine protocol to estimate changes in the SR Ca^{2+} load and found, like HT cells, no change in the caffeine-induced CaT amplitude observed in both models of caveolae disruption (Fig. 4E).

3.4. Inhibition of adenylyl cyclases prevents caveolae-mediated augmentation in Ca^{2+} spark activity

Previous studies linked caveolae to the spatial-temporal regulation of cAMP signaling in ventricular myocytes via localization of ACs and PDEs in caveolar microdomains [6]. To determine whether HT swelling affects cAMP signaling, we applied FRET imaging to wild-type rat ACMs transfected with either a plasma membrane-targeted (pmEPAC2) or cytosolic (cEPAC2 [9]) cAMP biosensors [14]. We found that HT challenge and disruption of caveolae by MβCD both resulted in a rise in cAMP level over the 15 mins of treatment (Fig. 5A, B). Cytosolic changes in FRET signal also demonstrated a significant elevation of cAMP level during both HT challenge and MβCD treatment after 10 mins (Fig. 6C, D).

To determine whether the re-distribution of cAMP production pattern contributes to the increase in CaSp activity observed in 3 models of caveolae disruption, we tested the impact

of AC inhibition by two non-selective antagonists MDL12330 [26] and SQ22536 [27]. While neither drug changed CaSp frequency in IT conditions (Fig. 5E), pre-incubation of ACMs with both MDL12330 and SQ22536 prevented the increase on CaSp frequency during HT challenge (Fig. 5F). Inhibition of ACs also significantly decreased CaSp frequency in MβCD-treated (Fig. 5G) and Cav3KO cells (Fig. 5H). These findings suggest a key role of ACs in caveolae-mediated re-distribution of cAMP production in stretch-induced augmentation of CaSp activity.

3.5. Caveolae disruption augments RyR phosphorylation at PKA specific sites

Increase in cAMP production observed during caveolae disruption could subsequently contribute to phosphorylation of cytosolic proteins, including RyRs [28]. To examine this further, we used immunofluorescent labeling with phospho-specific RyR2 antibodies: RyR2-Ser^{2030} for PKA phosphorylation site [23], RyR2-Ser^{2808} for both PKA and CaMKII phosphorylation site, and RyR2-Ser^{2814} CaMKII-specific phosphorylation site [29]. We analyzed the amount of total RyR2 overlaid with phospho-specific antibodies as a measure of RyR2 phosphorylation. In control experiments, we treated ACMs with (1) 100 nM isoproterenol to stimulate kinase activities, or (2) with H-89 and KN93 to inhibit PKA and CaMKII activities, respectively. Figs. S1–S3 show that, for all three phosphorylation sites, the application of isoproterenol significantly increased the level of RyR2 phosphorylation, whereas incubation with H-89 and KN93 significantly reduced this parameter.

WT and Cav3KO ACMs treated with IT, HT conditions, as well as after MβCD treatment, were then labeled with total RyR2 and one of the phosphorylated-specific sites (Fig. 6). Co-localization analysis of total versus phosphorylated RyR2 demonstrated a significant increase of pRyR2-Ser^{2030} (Fig. 6A) and pRyR2-Ser^{2808} (Fig. 6B) for all three models of caveolae loss which indicates an upregulation of cytosolic PKA activity after caveolae disruption. Interestingly, pRyR2-Ser^{2814} level did not change in HT and MβCD cells and decreased in Cav3KO myocytes (Fig. 6C).

Distribution of pRyR2-Ser^{2030} phosphorylation was analyzed near the surface sarcolemma and in the cytosol (Fig. 6D). In control cells, we found significantly higher levels of pRyR2-Ser^{2030} located close to sarcolemma vs. cytosol (Fig. 6E). In HT cells, this difference disappeared, likely due to significant elevation of pRyR2-Ser^{2030} in the cytosol. Similar to augmentation of Ca^{2+} signaling during HT protocol (Fig. 3), pRyR2-Ser^{2808} phosphorylation was also transiently increased during swelling, with initial increase at 1–2 min followed by a significant reduction at 8 min of HT challenge (Fig. 6F).

To translate the observed findings into changes in Ca^{2+} signaling, CaSp frequency was measured when one of the kinases was inhibited: in the presence of PKA inhibitor H-89, or CaMKII inhibitor KN93 (Fig. 7A). In the setting of HT challenge, PKA inhibitor H-89 dramatically reduced CaSp frequency as compared with untreated cells (Fig. 7B), while during HT protocol KN93 did not change CaSp frequency when compared with either KN92 treatment or control cells (Fig. 7C).

3.6. Modelling of cAMP dynamics after caveolae loss

To investigate the effects of mechanically-induced caveolae disruption on mouse ACMs, we used our novel compartmentalized model of mouse ACM which combines the action potential (AP), CaT, and cAMP signaling, described in a microdomain-specific manner [13]. As we observed ~60% of caveolae density reduction during both *ex vivo* and *in vitro* stretch (Figs. 1E and 2D), we tested potential impacts of the single caveolar protein modifications in the caveolae compartment on the cAMP levels (Fig. 8B). These modifications include: (1) an increase in the cAMP flux from the caveolar to extracaveolar compartment by 5-fold; (2) a redistribution of 60% of the L-type Ca^{2+} channels from the caveolar to extracaveolar compartment; (3) a redistribution of 60% of β_2-adrenergic receptors and G_s from the caveolar to extracaveolar compartment; (4) a redistribution of 60% of AC5/6 from the caveolar to extracaveolar compartment; and (5) an inhibition of 100% PDE2, PDE3, and PDE4 in the caveolar compartment. For each of these modifications, we calculated the changes in cAMP concentration after 10 min in caveolae (Fig. 8Ai), extracaveolae (Fig. 8Aii) and cytosol (Fig. 8Aiii). Among all the simulations performed, only inhibition of caveolar PDEs induced a significant elevation of cAMP concentration in all microdomains (Fig. 8B). We further tested whether PDE inhibition can enhance CaSp activity in isolated ACMs *in vitro* (Fig. 8C). We found that cilostazol (PDE3 inhibitor) did not affect CaSp frequency, while rolipram (PDE4 inhibitor) and IBMX (nonselective PDE inhibitor) significantly elevated CaSp frequency. Thus, our model with PDEs inhibition in caveolae suggests that redistribution/loss of PDEs control of cAMP could be one of the main parts of the observed cAMP and Ca^{2+} augmentation after caveolae disruption.

Importantly, using computational modeling, we confirmed that caveolae-specific PDE inhibition leads to significant augmentation of CaT amplitude (Fig. 8D), as it was observed in isolated ACMs (Fig. 2C). Computational modeling also demonstrated that the observed changes in cAMP and Ca^{2+} signaling were associated with AP duration prolongation (Fig. 8E), as it was further confirmed by AP measurements in isolated ACMs during HT protocol (Fig. 8F and Fig. S4).

4. Discussion

4.1. Caveolae as mechanosensors

The ability to sense membrane forces may underlie many of the caveolae functions in diverse cell types, including endothelial, smooth muscle, and cardiac muscle cells. Sinha and colleagues [30] have shown that uniaxial stretch or osmotic swelling in different cell types caused a reversible loss of caveolae within minutes. They proposed that stretch-induced recruitment and flattening of caveolae buffers an increased membrane tension during cell stretch. Similarly, Kohl et al. observed myocyte membrane unfolding and incorporation of sub-sarcolemmal caveolae into the plasma membrane in loaded ventricles [31]. Similar experiments were performed by Pfeiffer et al. [32] on Langendorff-perfused mouse hearts where ventricular volume overload quickly (<1 min) and reversibly recruited caveolae to the sarcolemma. Importantly, in latter study, stretch-induced decrease in caveolar density coincided with conduction velocity slowing, and this effect was lost when caveolae were abolished by MβCD or Cav3KO, highlighting a crucial role of caveolae

in cardiomyocyte mechanotransduction and electrophysiology. Our findings from caveolae degradation in AMCs align with the results of previous studies and highlight caveolae-mediated cAMP/PKA/RyR2 axis as a part of cardiac mechanotransduction pathway.

4.2. Molecular mechanisms of mechano-chemical signal transduction

In cardiomyocytes, caveolae orchestrate a variety of signaling pathways, including spatial-temporal control of intracellular cAMP pools. From highly controlled signals with intact caveolae, cAMP pools are converted to a global cell-wide pattern when caveolae are disrupted [7,9]. We observed that caveolae loss induces an elevation of cAMP signal in both sarcolemma and cytosol (Fig. 5). We further confirmed that elevation in cytosolic cAMP level is responsible for increase in CaSp activity, as pre-treatment of cells with AC inhibitors prevented upregulation of CaSp in all models of caveolae disruption (Fig. 5E–H).

We next linked the caveolae-mediated increase in CaSp activity to PKA-induced phosphorylation of RyR2s. Similarly, an enhanced PKA-specific phosphorylation of SR phospholamban was previously observed after caveolae degradation [6]. Specifically, we showed transiently elevated levels of RyR2s phosphorylated at Ser^{2030} and Ser^{2808}, both PKA phosphorylation sites, after caveolae disruption and unchanged levels of Ser^{2814}, which is a CaMKII-specific residue (Fig. 6). There are some discrepancies in literature regarding the role of Ser^{2808} phosphorylation in the activation of CaSp. Some authors suggest Ser^{2808} as the main PKA-related phosphorylation site for RyR2s [33], while others did not find the activation of Ca^{2+} leak with Ser^{2808} phosphorylation in mouse ventricular myocytes [34,35]. Alternatively, Ser^{2030} was proposed as the main regulator for PKA-mediated Ca^{2+} leak from RyR2s [36–38]. Overall, we demonstrated that caveolae-induced increase in CaSp activity was lost when ACMs were pre-treated with PKA inhibitor H-89, supporting a crucial role of PKA activation and PKA-mediated regulation of Ca^{2+} handing proteins in stretch-induced augmentation of Ca^{2+} signaling.

Interestingly, we found that, under control conditions, phosphorylation of RyR2 at Ser^{2030} was significantly higher beneath the surface membrane compared to the cell interior (Fig. 6D, E). Such pattern could be associated with lack of developed T-tubular system in mouse ACMs [5,16], where phosphorylated RyR2s would be linked with caveolar cAMP compartments near the surface membrane. With disrupted caveolae, the spatial control of cAMP would be lost, resulting in upregulation of pRyR2-Ser^{2030} in the cytosol.

Our computational modeling provided additional details for the caveolae disruption mediated cAMP redistribution. While the effects of redistribution from caveolae to extra-caveolae compartments on cAMP levels, modeled for β_2-adrenergic receptors with G_s, L-type Ca^{2+} channels, and AC, were mild, inhibition of PDEs led to the most prominent elevation of cAMP in all compartments (Fig. 8A). This could be supported by the data from Yang and Scarlata, who demonstrated that swelling-induced flattening of caveolae structures does not affect the organization and membrane localization of the membrane components of caveolar macromolecular complexes, such as $G\alpha_i$-β_2 adrenoreceptor components [39]. It was also shown that swelling does not induce a translocation of Cav3 from caveolae to non-caveolae membrane fraction [17]. In contrast to the membrane-bound proteins, PDEs are mostly soluble proteins [40] and linked to caveolae compartment through the A kinase

anchoring proteins [41]. Therefore, caveolae loss could cause PDE uncoupling from the sarcolemma and their redistribution from native caveolar location to the cell interior. This would remove the cAMP sequestration and spatial control of cAMP signaling, leading to cAMP diffusion into other compartments and cAMP/PKA-mediated increase in CaSp activity, as it was mimicked by PDE4 inhibition in Fig. 8C. Thus, we propose that PDEs inhibition may be one of the main factors contributing to the alterations of Ca^{2+} handling during cardiomyocyte stretch.

4.3. Stretch and atrial arrhythmogenesis

Myocardial stretch has previously been linked to the development of atrial fibrillation (AF) [12,42], the most common cardiac rhythm disorder. Clinically, AF often occurs in the setting of atrial distension [43] associated with chronically elevated atrial pressure/volume overload and pathological cardiomyocyte stretch. On the cellular level, AF triggers have been linked to hyperactivity of RyR2s [29,44], which results in Ca^{2+} leak from the SR, augmentation of Na^{+}/Ca^{2+}-exchanger and development of the arrhythmogenic delayed afterdepolarizations [44]. In patients with paroxysmal AF, leaky RyR2s have been associated with upregulated PKA activity and PKA-mediated hyperphosphorylation or RyR2s [29], as it was also observed in the present study under caveolae disruption. This mechanism is in line with recent finding from human AF myocytes, where downregulation of PDE4 was linked to elevated cAMP level, increase in CaSp activity, and the incidence of arrhythmias [45]. It is also supported by our previous findings that stretch significantly potentiates adrenergically-driven arrhythmogenesis in rat pulmonary veins [19].

4.4. Study limitations

In the present study, to model stretch-induced decrease in caveolae density observed in *ex vivo* atria during overload, we utilized three *in vitro* protocols of caveolae disruption in isolated cardiomyocytes, including (1) mechanical disruption via HT swelling, (2) cholesterol depletion, and (3) Cav3KO. While all these models shared the effects associated with caveolae disruption, including augmentation of cAMP signaling, cAMP-mediated increase in PKA activity, PKA-mediated phosphorylated RyRs, and elevation of Ca^{2+} spark activity, it is possible that each protocol of caveolae disruption induces additional effects on cardiomyocyte electrophysiology which were not the focus of this study. Furthermore, cardiomyocyte stretch, including HT swelling, could directly modulate biophysical properties of various ion channels affecting AP morphology [46]. The exact mechanisms of such mechano-electrical feedback regulation remain poorly understood and would require additional investigations. Finally, while our computational studies suggested that a decrease in caveolar PDE activity results from caveolae disruption, future experiments are required to test this hypothesis.

5. Conclusions

Our findings add a new dimension to cardiac mechanobiology and highlight caveolae-associated cAMP/PKA-mediated phosphorylation of Ca^{2+} handling proteins as a novel component of mechano-chemical feedback in ACMs. Our results also indicate a transient nature of stretch-mediated modulation of Ca^{2+} signaling that may include a

few counteracting subcellular targets as well as complex spatial-temporal interactions between different components of mechano-chemical signal transduction. A comprehensive understanding of this autoregulatory signaling pathway is critical to advance our knowledge on plasticity of atrial myocardium. Its resilience to elevated hemodynamic pressure and volume overload observed during pathological conditions and associated with atrial remodeling and arrhythmogenesis.

Supplementary Material

Refer to Web version on PubMed Central for supplementary material.

Acknowledgements

Funding for this study was provided by the American Heart Association (16SDG29120011 to AVG, 915335 to RYM, 903203 to DGPT, and 846898 and 17POST33370089 to DL), the Wisconsin Partnership Program (4140 to AVG), the University of Wisconsin-Madison Office of the Vice Chancellor for Research and Graduate Education (DGPT), the Hilldale Undergraduate Research Fellowship (FCD), and the National Institutes of Health (from R01HL141214, R01HL139738, R01HL146652 to AVG, R01HL161070 to FJA, and T32GM008688 to DGPT). Last, we thank Randall J. Massey and the SMPH Electron Microscopy Facility (University of Wisconsin-Madison) for critical assistance in preparing and imaging atrial myocyte.

Data availability

The datasets generated during and/or analyzed during the current study are available from the corresponding author on reasonable request.

References

[1]. Parton RG, Simons K, The multiple faces of caveolae, Nat. Rev. Mol. Cell Biol 8 (2007) 185–194. 10.1038/nrm2122. [PubMed: 17318224]

[2]. Trafford AW, Clarke JD, Richards MA, Eisner DA, Dibb KM, Calcium signalling microdomains and the t-tubular system in atrial mycoytes: Potential roles in cardiac disease and arrhythmias, Cardiovasc. Res 98 (2013) 192–203. 10.1093/cvr/cvt018. [PubMed: 23386275]

[3]. Glukhov AV, Balycheva M, Sanchez-Alonso JL, Ilkan Z, Alvarez-Laviada A, Bhogal N, Diakonov I, Schobesberger S, Sikkel MB, Bhargava A, Faggian G, Punjabi PP, Houser SR, Gorelik J, Direct Evidence for Microdomain-Specific Localization and Remodeling of Functional L-Type Calcium Channels in Rat and Human Atrial Myocytes, Circulation. 132 (2015) 2372–2384. 10.1161/CIRCULATIONAHA.115.018131. [PubMed: 26450916]

[4]. Gabella G, Inpocketings of the cell membrane (caveolae) in the rat myocardium, J. Ultrasructure Res 65 (1978) 135–147. 10.1016/S0022-5320(78)90051-5.

[5]. Smyrnias I, Mair W, Harzheim D, Walker SA, Roderick HL, Bootman MD, Comparison of the T-tubule system in adult rat ventricular and atrial myocytes, and its role in excitation–contraction coupling and inotropic stimulation, Cell Calcium. 47 (2010) 210–23. 10.1016/j.ceca.2009.10.001. [PubMed: 20106523]

[6]. Calaghan S, Kozera L, White E, Compartmentalisation of cAMP-dependent signalling by caveolae in the adult cardiac myocyte, J. Mol. Cell. Cardiol 45 (2008) 88–92. 10.1016/j.yjmcc.2008.04.004. [PubMed: 18514221]

[7]. MacDougall DA, Agarwal SR, Stopford EA, Chu H, Collins JA, Longster AL, Colyer J, Harvey RD, Calaghan S, Caveolae compartmentalise β_2-adrenoceptor signals by curtailing cAMP production and maintaining phosphatase activity in the sarcoplasmic reticulum of the adult ventricular myocyte, J. Mol. Cell. Cardiol 52 (2012) 388–400. 10.1016/j.yjmcc.2011.06.014. [PubMed: 21740911]

[8]. Balijepalli RC, Foell JD, Hall DD, Hell JW, Kamp TJ, Localization of cardiac L-type Ca^{2+} channels to a caveolar macromolecular signaling complex is required for β_2-adrenergic regulation, Proc. Natl. Acad. Sci. U.S.A 103 (2006) 7500–7505. 10.1073/pnas.0503465103. [PubMed: 16648270]

[9]. Nikolaev VO, Moshkov A, Lyon AR, Miragoli M, Novak P, Paur H, Lohse MJ, Korchev YE, Harding SE, Gorelik J, β_2-Adrenergic Receptor Redistribution in Heart Failure Changes cAMP Compartmentation, Science. 327 (2010) 1653–1657. 10.1126/science.1185988. [PubMed: 20185685]

[10]. Wright PT, Nikolaev VO, O'Hara T, Diakonov I, Bhargava A, Tokar S, Schobesberger S, Shevchuk AI, Sikkel MB, Wilkinson R, Trayanova NA, Lyon AR, Harding SE, Gorelik J, Caveolin-3 regulates compartmentation of cardiomyocyte beta2-adrenergic receptor-mediated cAMP signaling, J. Mol. Cell. Cardiol 67 (2014) 38–48. 10.1016/j.yjmcc.2013.12.003. [PubMed: 24345421]

[11]. Haque MZ, McIntosh VJ, Samra ABA, Mohammad RM, Lasley RD, Cholesterol depletion alters cardiomyocyte subcellular signaling and increases contractility, PLoS One. 11 (2016) e0154151. 10.1371/journal.pone.0154151. [PubMed: 27441649]

[12]. Ravelli F, Allessie M, Effects of atrial dilatation on refractory period and vulnerability to atrial fibrillation in the isolated Langendorff-perfused rabbit heart, Circulation. 96 (1997) 1686–1695. 10.1161/01.CIR.96.5.1686. [PubMed: 9315565]

[13]. Asfaw TN, Tyan L, Glukhov AV, Bondarenko VE, A compartmentalized mathematical model of mouse atrial myocytes, Am. J. Physiol. Heart Circ. Physiol 318 (2020) H485–H507. 10.1152/ajpheart.00460.2019. [PubMed: 31951471]

[14]. Wright PT, Bhogal NK, Diakonov I, Pannell LMK, Perera RK, Bork NI, Schobesberger S, Lucarelli C, Faggian G, Alvarez-Laviada A, Zaccolo M, Kamp TJ, Balijepalli RC, Lyon AR, Harding SE, Nikolaev VO, Gorelik J, Cardiomyocyte Membrane Structure and cAMP Compartmentation Produce Anatomical Variation in β_2AR-cAMP Responsiveness in Murine Hearts, Cell Rep. 23 (2018) 459–469. 10.1016/j.celrep.2018.03.053. [PubMed: 29642004]

[15]. Tyan L, Turner D, Komp KR, Medvedev RY, Lim E, V Glukhov A, Caveolin-3 is required for regulation of transient outward potassium current by angiotensin II in mouse atrial myocytes, Am. J. Physiol. - Hear. Circ. Physiol 320 (2021) H787–H797. 10.1152/ajpheart.00569.2020.

[16]. Lang D, Medvedev RY, Ratajczyk L, Zheng J, Yuan X, Lim E, Han OY, Valdivia HH, V Glukhov A, Region-specific distribution of transversal-axial tubule system organization underlies heterogeneity of calcium dynamics in the right atrium, Am. J. Physiol. - Hear. Circ. Physiol 322 (2022) H269–H284. 10.1152/AJPHEART.00381.2021.

[17]. Kozera L, White E, Calaghan S, Caveolae Act as Membrane Reserves Which Limit Mechanosensitive $I_{Cl,swell}$ Channel Activation during Swelling in the Rat Ventricular Myocyte, 4 (2009) e8312. 10.1371/journal.pone.0008312.

[18]. Wei EQ, Sinden DS, Mao L, Zhang H, Wang C, Pitt GS, Inducible Fgf13 ablation enhances caveolae-mediated cardioprotection during cardiac pressure overload, Proc. Natl. Acad. Sci. U.S.A 114 (2017) E4010–E4019. 10.1073/pnas.1616393114. [PubMed: 28461495]

[19]. Egorov YV, Lang D, Tyan L, Turner D, Lim E, Piro ZD, Hernandez JJ, Lodin R, Wang R, Schmuck EG, Raval AN, Ralphe CJ, Kamp TJ, Rosenshtraukh LV, V Glukhov A, Caveolae-Mediated Activation of Mechanosensitive Chloride Channels in Pulmonary Veins Triggers Atrial Arrhythmogenesis, J. Am. Heart Assoc 8 (2019) e012748. 10.1161/JAHA.119.012748. [PubMed: 31597508]

[20]. Medvedev R, Sanchez-Alonso JL, Alvarez-Laviada A, Rossi S, Dries E, Schorn T, Abdul-Salam VB, Trayanova N, Wojciak-Stothard B, Miragoli M, Faggian G, Gorelik J, Nanoscale Study of Calcium Handling Remodeling in Right Ventricular Cardiomyocytes Following Pulmonary Hypertension, Hypertension. 77 (2021) 605–616. 10.1161/HYPERTENSIONAHA.120.14858. [PubMed: 33356404]

[21]. Picht E, Zima AV, Blatter LA, Bers DM, SparkMaster: automated calcium spark analysis with ImageJ, AJP Cell Physiol. 293 (2007) C1073–C1081. 10.1152/ajpcell.00586.2006.

[22]. Medvedev RY, Sanchez-Alonso JL, Mansfield CA, Judina A, Francis AJ, Pagiatakis C, Trayanova N, V Glukhov A, Miragoli M, Faggian G, Gorelik J, Local hyperactivation of L-type Ca^{2+} channels increases spontaneous Ca^{2+} release activity and cellular hypertrophy

in right ventricular myocytes from heart failure rats, Sci. Rep 11 (2021) 4840. 10.1038/s41598-021-84275-w. [PubMed: 33649357]

[23]. Benkusky NA, Weber CS, Scherman JA, Farrell EF, Hacker TA, John MC, Powers PA, Valdivia HH, Intact β-adrenergic response and unmodified progression toward heart failure in mice with genetic ablation of a major protein kinase A phosphorylation site in the cardiac ryanodine receptor, Circ. Res 101 (2007) 819–829. 10.1161/CIRCRESAHA.107.153007. [PubMed: 17717301]

[24]. Fletcher PA, Scriven DRL, Schulson MN, Moore EDW, Multi-image colocalization and its statistical significance, Biophys. J 99 (2010) 1996–2005. 10.1016/j.bpj.2010.07.006. [PubMed: 20858446]

[25]. Gonano LA, Morell M, Burgos JI, Dulce RA, De Giusti VC, Aiello EA, Hare JM, Petroff MV, Hypotonic swelling promotes nitric oxide release in cardiac ventricular myocytes: Impact on swelling-induced negative inotropic effect, Cardiovasc. Res 104 (2014) 456–466. 10.1093/cvr/cvu230. [PubMed: 25344365]

[26]. Collins TP, Terrar DA, Ca^{2+}-stimulated adenylyl cyclases regulate the L-type Ca^{2+} current in guinea-pig atrial myocytes, J. Physiol 590 (2012) 1881–1893. 10.1113/jphysiol.2011.227066. [PubMed: 22351635]

[27]. Brand CS, Hocker HJ, Gorfe AA, Cavasotto CN, Dessauer CW, Isoform selectivity of adenylyl cyclase inhibitors: Characterization of known and novel compounds, J. Pharmacol. Exp. Ther 347 (2013) 265–275. 10.1124/jpet.113.208157. [PubMed: 24006339]

[28]. Pereira L, Cheng H, Lao DH, Na L, Van Oort RJ, Brown JH, Wehrens XHT, Chen J, Bers DM, Epac2 mediates cardiac β_1-adrenergic-dependent sarcoplasmic reticulum Ca^{2+} leak and arrhythmia, Circulation. 127 (2013) 913–922. 10.1161/CIRCULATIONAHA.12.148619. [PubMed: 23363625]

[29]. Voigt N, Li N, Wang Q, Wang W, Trafford AW, Abu-Taha I, Sun Q, Wieland T, Ravens U, Nattel S, Wehrens XHT, Dobrev D, Enhanced sarcoplasmic reticulum Ca2+ Leak and increased Na^{+}-Ca^{2+} exchanger function underlie delayed afterdepolarizations in patients with chronic atrial fibrillation, Circulation. 125 (2012) 2059–2070. 10.1161/CIRCULATIONAHA.111.067306. [PubMed: 22456474]

[30]. Sinha B, Köster D, Ruez R, Gonnord P, Bastiani M, Abankwa D, Stan RV, Butler-Browne G, Vedie B, Johannes L, Morone N, Parton RG, Raposo G, Sens P, Lamaze C, Nassoy P, Cells respond to mechanical stress by rapid disassembly of caveolae, Cell. 144 (2011) 402–413. 10.1016/j.cell.2010.12.031. [PubMed: 21295700]

[31]. Kohl P, Cooper PJ, Holloway H, Effects of acute ventricular volume manipulation on in situ cardiomyocyte cell membrane configuration, Prog. Biophys. Mol. Biol 82 (2003) 221–227. 10.1016/S0079-6107(03)00024-5. [PubMed: 12732281]

[32]. Pfeiffer ER, Wright AT, Edwards AG, Stowe JC, McNall K, Tan J, Niesman I, Patel HH, Roth DM, Omens JH, McCulloch AD, Caveolae in ventricular myocytes are required for stretch-dependent conduction slowing, J. Mol. Cell. Cardiol 76 (2014) 265–274. 10.1016/j.yjmcc.2014.09.014. [PubMed: 25257915]

[33]. Bovo E, Huke S, Blatter LA, Zima AV, The effect of PKA-mediated phosphorylation of ryanodine receptor on SR Ca^{2+} leak in ventricular myocytes, J. Mol. Cell. Cardiol 104 (2017) 9–16. 10.1016/j.yjmcc.2017.01.015. [PubMed: 28131630]

[34]. Li Y, Kranias EG, Mignery GA, Bers DM, Protein kinase A phosphorylation of the ryanodine receptor does not affect calcium sparks in mouse ventricular myocytes, Circ. Res 90 (2002) 309–316. 10.1161/hh0302.105660. [PubMed: 11861420]

[35]. Zhang H, Makarewich CA, Kubo H, Wang W, Duran JM, Li Y, Berretta RM, Koch WJ, Chen X, Gao E, Valdivia HH, Houser SR, Hyperphosphorylation of the cardiac ryanodine receptor at serine 2808 is not involved in cardiac dysfunction after myocardial infarction, Circ. Res 110 (2012) 831–840. 10.1161/CIRCRESAHA.111.255158. [PubMed: 22302785]

[36]. Xiao B, Tian X, Xie W, Jones PP, Cai S, Wang X, Jiang D, Kong H, Zhang L, Chen K, Walsh MP, Cheng H, Chen SRW, Functional Consequence of Protein Kinase A-dependent Phosphorylation of the Cardiac Ryanodine Receptor, J. Biol. Chem 282 (2007) 30256–30264. 10.1074/jbc.m703510200. [PubMed: 17693412]

[37]. Wang Y, Li C, Shi L, Chen X, Cui C, Huang J, Chen B, Hall DD, Pan Z, Lu M, Hong J, Song LS, Zhao S, Integrin β_1D Deficiency-Mediated RyR2 Dysfunction Contributes to Catecholamine-Sensitive Ventricular Tachycardia in Arrhythmogenic Right Ventricular Cardiomyopathy, Circulation. 141 (2020) 1477–1493. 10.1161/CIRCULATIONAHA.119.043504. [PubMed: 32122157]

[38]. Potenza DM, Janicek R, Fernandez-Tenorio M, Camors E, Ramos-Mondragón R, Valdivia HH, Niggli E, Phosphorylation of the ryanodine receptor 2 at serine 2030 is required for a complete β-adrenergic response, J. Gen. Physiol 151 (2019) 131–145. 10.1085/JGP.201812155. [PubMed: 30541771]

[39]. Yang L, Scarlata S, Super-resolution visualization of caveola deformation in response to osmotic stress, J. Biol. Chem 292 (2017) 3779–3788. 10.1074/jbc.M116.768499. [PubMed: 28096469]

[40]. Mika D, Leroy JÔ, Vandecasteele G, Fischmeister R, PDEs create local domains of cAMP signaling, J. Mol. Cell. Cardiol 52 (2012) 323–329. 10.1016/j.yjmcc.2011.08.016. [PubMed: 21888909]

[41]. Logue JS, Scott JD, Organizing signal transduction through A-kinase anchoring proteins (AKAPs), FEBS J. 277 (2010) 4370–4375. 10.1111/j.1742-4658.2010.07866.x. [PubMed: 20883492]

[42]. Fedorov VV, Trifonova OP, Glukhov AV, Rosen MR, Rosenshtraukh LV., The Role of Mechano-Electrical Feedback in the Cholinergic Atrial Fibrillation Initiation, Academia, 2005.

[43]. Benjamin EJ, Levy D, Vaziri SM, D'agostino RB, Belanger AJ, Wolf PA, Independent Risk Factors for Atrial Fibrillation in a Population-Based Cohort: The Framingham Heart Study, JAMA. 271 (1994) 840–844. 10.1001/JAMA.1994.03510350050036. [PubMed: 8114238]

[44]. Heijman J, Voigt N, Nattel S, Dobrev D, Cellular and molecular electrophysiology of atrial fibrillation initiation, maintenance, and progression, Circ. Res 114 (2014) 1483–1499. 10.1161/CIRCRESAHA.114.302226. [PubMed: 24763466]

[45]. Molina CE, Leroy J, Richter W, Xie M, Scheitrum C, Lee IO, Maack C, Rucker-Martin C, Donzeau-Gouge P, Verde I, Llach A, Hove-Madsen L, Conti M, Vandecasteele G, Fischmeister R, Cyclic adenosine monophosphate phosphodiesterase type 4 protects against atrial arrhythmias, J. Am. Coll. Cardiol 59 (2012) 2182–2190. 10.1016/j.jacc.2012.01.060. [PubMed: 22676938]

[46]. Peyronnet R, Nerbonne JM, Kohl P, Cardiac Mechano-Gated Ion Channels and Arrhythmias, Circ. Res 118 (2016) 311–329. 10.1161/CIRCRESAHA.115.305043. [PubMed: 26838316]

Highlights

- Caveolae represent an important component of membrane mechanosensing and mechanical regulation of cellular function, while their role in cardiac mechanotransduction is poorly understood.
- Stretching of atrial myocytes flattens caveolae and increases membrane tension.
- Caveolae disruption via elevated membrane tension, cholesterol depletion or cardiac-specific genetic deletion of caveolar scaffolding protein caveolin-3, results in temporal augmentation of Ca^{2+} signaling through cAMP-mediated increase in PKA-phosphorylated ryanodine receptors.
- Computational modeling linked the observed changes in Ca^{2+} signaling to a loss of caveolae-confined control of cAMP signaling by phosphodiesterases.
- Our findings highlight caveolae-associated cAMP/PKA-mediated phosphorylation of Ca^{2+} handling proteins as a novel component of mechano-chemical feedback in atrial cardiomyocytes.

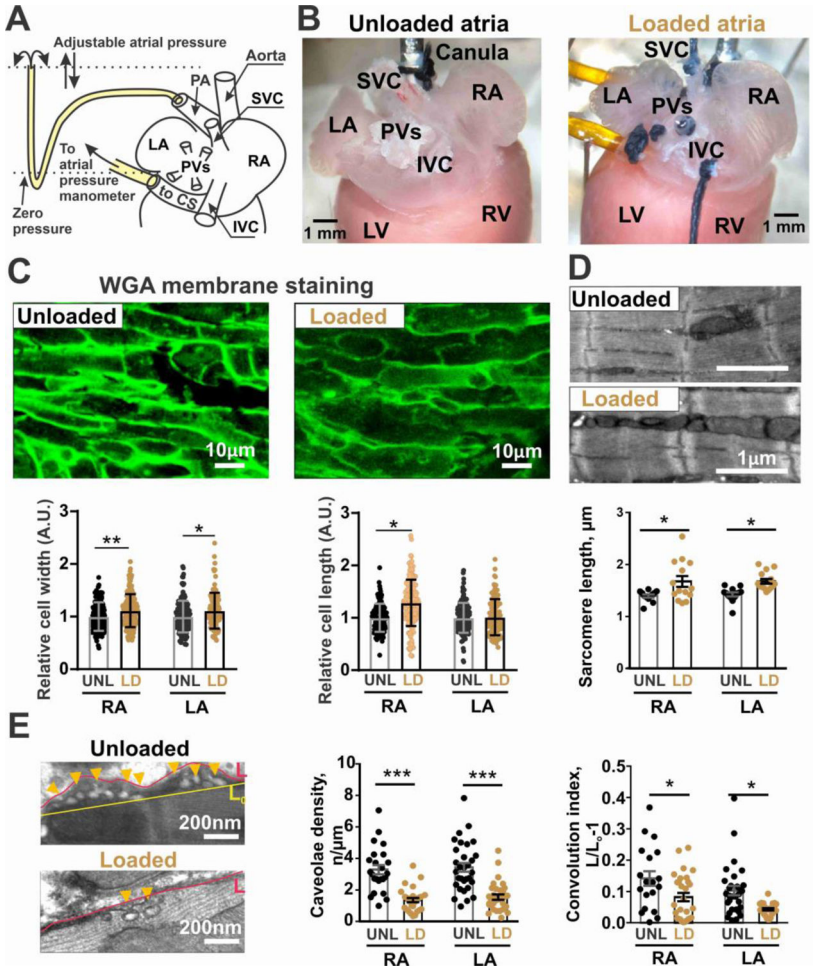

Fig. 1. Atrial volume overload causes ACM stretch and caveolae degradation.

(A) Schematic of the *ex vivo* atrial volume overload protocol. (B) Photographs of unloaded (UNL, *left*) and loaded (LD, *right*) mouse hearts. (C) WGA-stained atrial sections from unloaded and loaded ex *vivo* hearts are shown together with the relative changes in cell width and length in right (RA) and left (LA) ACMs. n=120/180 RA-UNL/LD and n=140/70 LA-UNL/LD cells from N=3 mice. *,** – $p<0.05$, <0.01 by two-way ANOVA. (D) TEM microphotographs together with the average sarcomere length measured in RA and LA myocytes from unloaded and loaded atria. n=12/14 RA-UNL/LD and n=13/14 LA-UNL/LD cells from N=3 mice. * – $p<0.05$ by two-way ANOVA. (E) TEM microphotographs showing caveolae structures in unloaded and loaded atria (*left*), average caveolae density (*middle*) and membrane convolution index (*right*) from RA and LA cells. n=24/29 RA-UNL/LD and n=31/31 LA-UNL/LD cells from N=3 mice. *,*** – $p<0.05$, $p<0.001$ by two-way ANOVA.

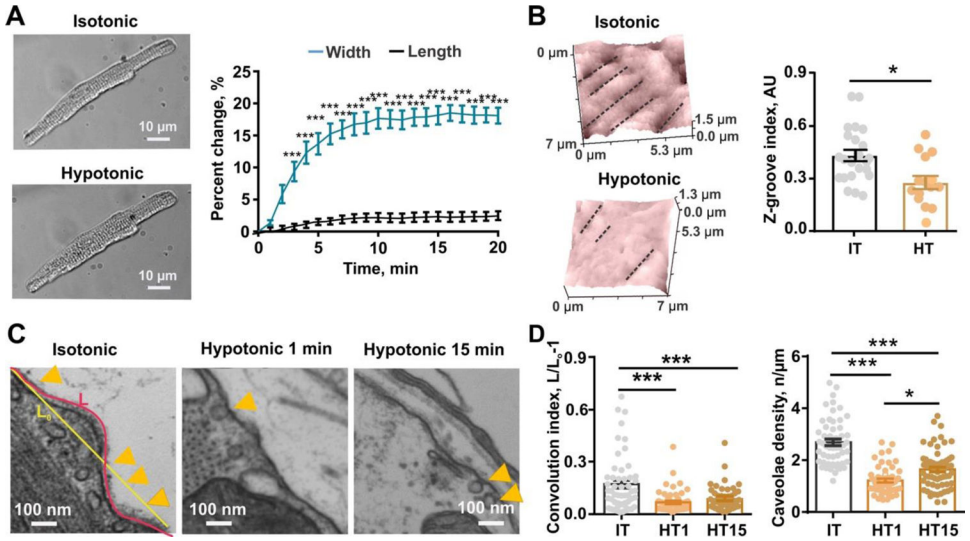

Fig. 2. Hypotonic stress induces changes in ACM morphology.

(A) Morphological changes of ACMs during hypotonic stress. Right: Relative changes in cell width and length are shown during hypotonic cell swelling over time. n=20 cells from N=3 mice. *** – p<0.001 by one-way ANOVA. (B) Left: Typical SICM topographical scans of ACMs at isotonic and hypotonic conditions. Right: Average Z-groove ratio under isotonic (IT) and hypotonic (HT) conditions. n=19 (IT) and n=13 (HT) from N=3 mice. * – p<0.05 by Student t test. (C) TEM micrographs demonstrate significant decrease in caveolae density (orange arrowheads). (D) Average data for membrane convolution index (*left*) and caveolae density (*right*) in ACMs under IT (n=51 cells), HT at 1 min (n=60 cells) vs. HT at 15 min (n=52 cells). *,*** – p<0.05, <0.001 by one-way ANOVA.

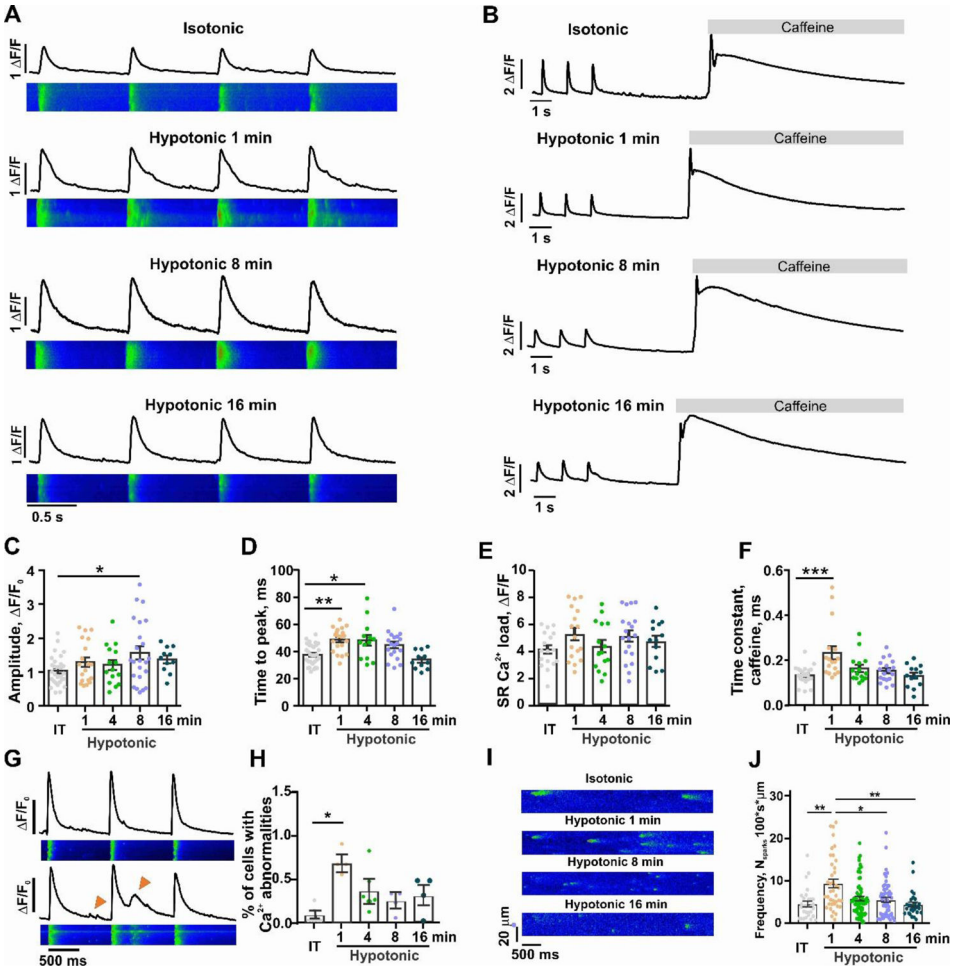

Fig. 3. Swelling-induced changes in ACM Ca^{2+} handling.

(A) Representative traces of Ca^{2+} transients (CaT) recorded at 1 Hz pacing in IT/HT buffers. (B) Representative traces of caffeine-induced CaTs in ACMs bathed in IT and different time points of HT solutions. (C-F), summary graphs showing changes in CaT amplitude (C), time to peak (D), caffeine-induced CaT amplitude (E) and CaT decay constant (K_{caf}) (F) measured during 1 Hz pacing at different time points of HT swelling. n=30 cells (IT), 19 (H1), 15 (H4), 23 (H8) and 12 (H16) from N=5 mice. *,** – $p<0.05$, <0.01 by two-way ANOVA. (G-H) Representative examples of abnormal Ca^{2+} oscillations in ACMs during HT (G, *bottom*) and average percentage of cells with CaT abnormalities at different times of HT swelling (H). n=5–7 cells/mice. Each dot represents a percentage of cells with Ca^{2+} abnormalities in one experimental day. * – $p<0.05$ by two-way ANOVA. (I) Typical linescans of Ca^{2+} sparks activity in ACMs treated with IT/HT buffers. (J) Summarized data for the frequency of Ca^{2+} sparks recorded in IT and at different time points of HT swelling. n=27 (IT), 15 (H1), 22 (H4), 18 (H8) and 21 (H16) from N=5 mice. *,** – $p<0.05$, $p<0.01$ vs. IT by two-way ANOVA.

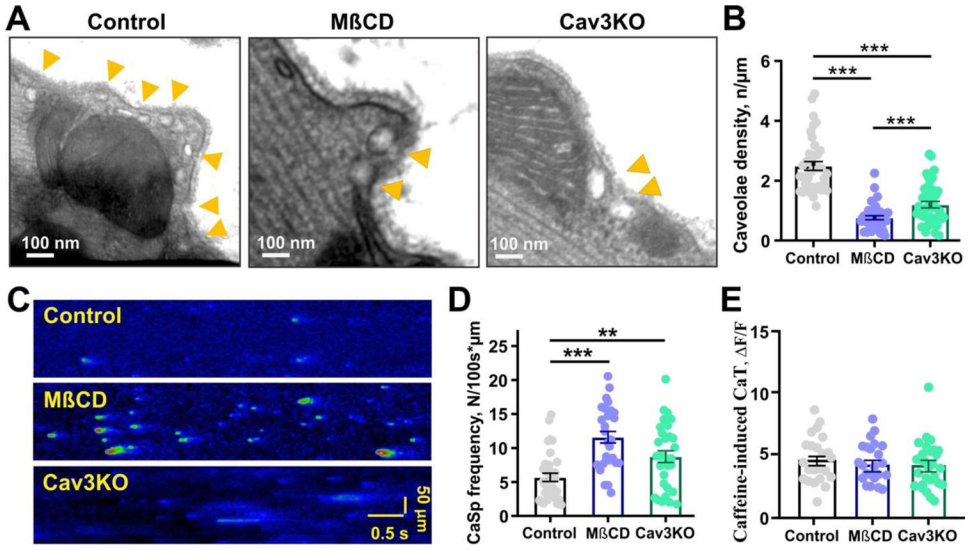

Fig. 4. Ca^{2+} activity in ACMs with disrupted caveolae.

(A) Representative TEM images of membrane structures from control, MβCD-treated WT, and Cav3KO ACMs. (B) Statistical analysis of caveolae density in control (n=39), MβCD-WT (40) and Cav3KO (n=41) ACMs. *** – p<0.001, by one-way ANOVA. (C) Representative linescans of Ca^{2+} spark activity and statistical analysis of Ca^{2+} spark frequency (D) recorded in control (n=32), MβCD-WT (n=28), and Cav3KO (n=29) ACMs. **, *** – p<0.01, 0.001 by one-way ANOVA. (E) Average data for caffeine-induced CaT amplitude in control (n=23), MβCD-WT (n=23), and Cav3KO (n=28) ACMs.

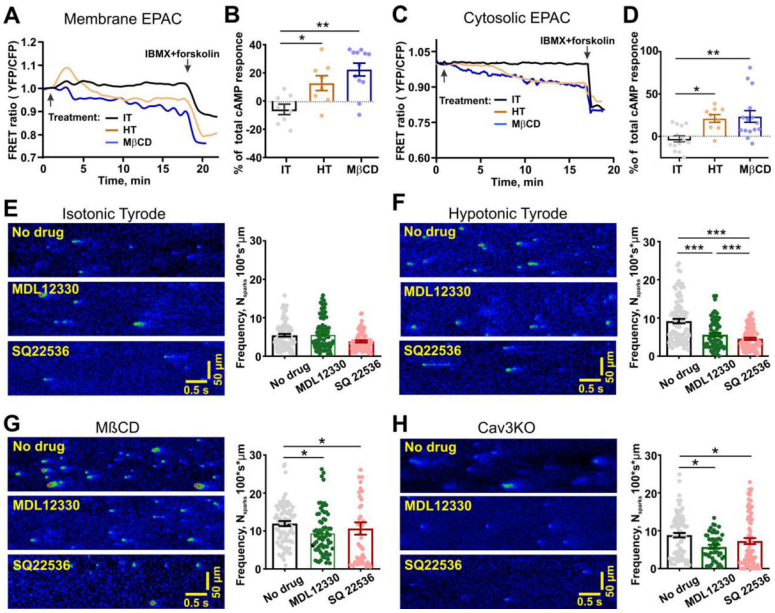

Fig. 5. Caveolae depletion induces fluxes of cAMP promoting CaSp activity.

(A) Average FRET traces showing the baseline, IT/HT/MβCD-induced (labeled as treatment) and full cAMP (IBMX + forskolin) responses measured using plasma membrane EPAC2 (pmEPAC) sensor in ACMs. (B) Average cAMP changes near the sarcolemma normalized by total cAMP signal induced by IT (n=8), HT (n=9) and MβCD (n=13) treatments. *,** – p<0.05, p<0.01 by one-way ANOVA. (C) Average FRET traces showing IT/HT/ MβCD-induced and full cAMP (saturator) responses of cytosolic cEPAC2 (cEPAC) sensor in ACMs. (D) Mean cAMP change normalized by total AC signal induced by IT (n=14)/HT (n=9)/MβCD (n=12) treatments. *, ** – p<0,05, 0.01 by one-way ANOVA. (E-H) Typical Ca^{2+} spark recordings (*left*) and summarized data for Ca^{2+} spark frequency (CaSpF, *right*) measured in ACMs with no treatment (n=31) and after MDL12330 (n=29) and SQ22536 (n=24) in IT (E), in HT (n=32/25/31 cells for no drug/MDL12330/SQ22536, F), after MβCD treatment (n=28/23/16 for no drug/MDL12330/SQ22536, G), and in Cav3KO ACMs (n=29/16/23 cells no drug/MDL12330/SQ22536, H). *,*** – p<0.05, 0.001 by one-way ANOVA.

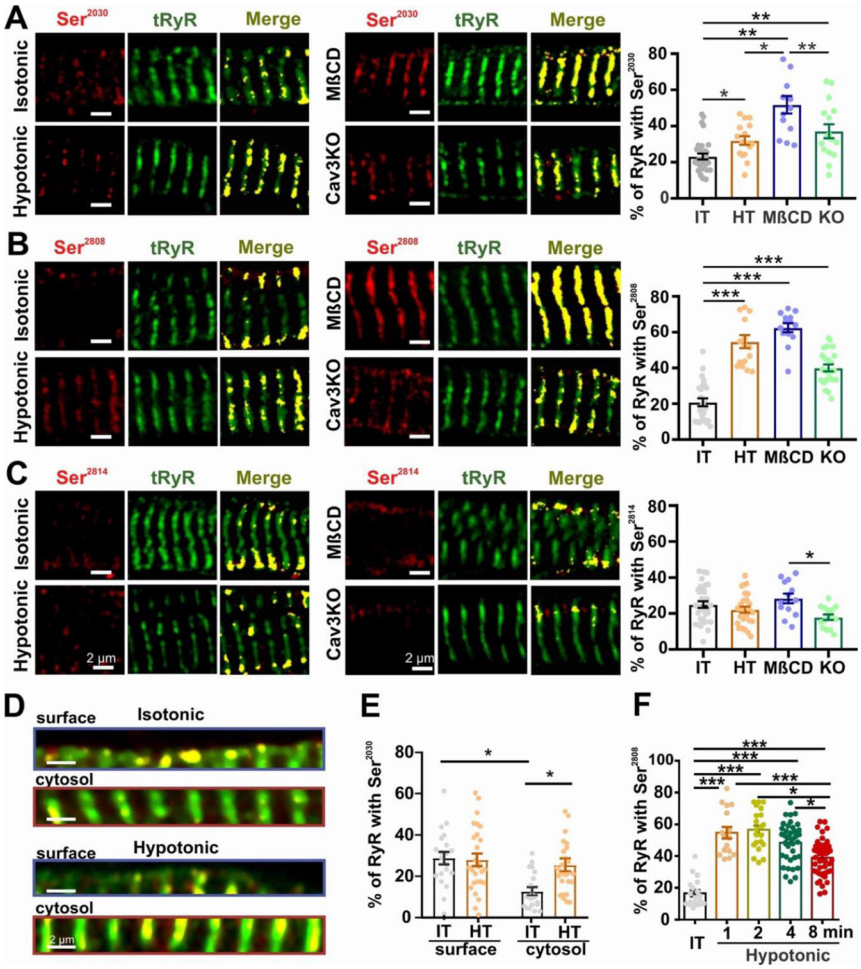

Fig. 6. Redistribution of PKA-phosphorylated RyR2s in stretched ACMs.

(A-C) Colocalization analysis for total (greed) and phospho-specific (red) RyR2 in WT ACM under isotonic (IT) and hypertonic (HT) conditions, MβCD-treated WT, and Cav3KO ACMs. Representative confocal images and colocalization analysis are shown for pRyR2-Ser^{2030} (n=39/18/13/16 cells for IT/HT 1 min/MβCD/Cav3KO groups, A), pRyR2-Ser^{2808} (n=25/16/14/24 cells for IT/HT 1 min/MβCD/Cav3KO groups, B), and pRyR2-Ser^{2814} (n=33/27/15/7 cells for IT/HT 1 min/MβCD/Cav3KO groups, C). *, **, *** – p<0.05, 0.01, <0.001 by one-way ANOVA. (D) Representative confocal sections with 30×1 μM selected near the sarcolemma (blue box) and in the cytosol (red box). (E) Graph of the corresponding colocalization analysis. N=22/16 IT/HT cells. *– p<0.05 by two-way ANOVA. (F) Time course of pRyR2-Ser^{2808}change during cell swelling. IT (n=39), HT: 1 min (n=16), 2 min (n=21), 4 min (n=30) and 8 min (n=45). *, *** – p<0.05, 0.001 by one-way ANOVA.

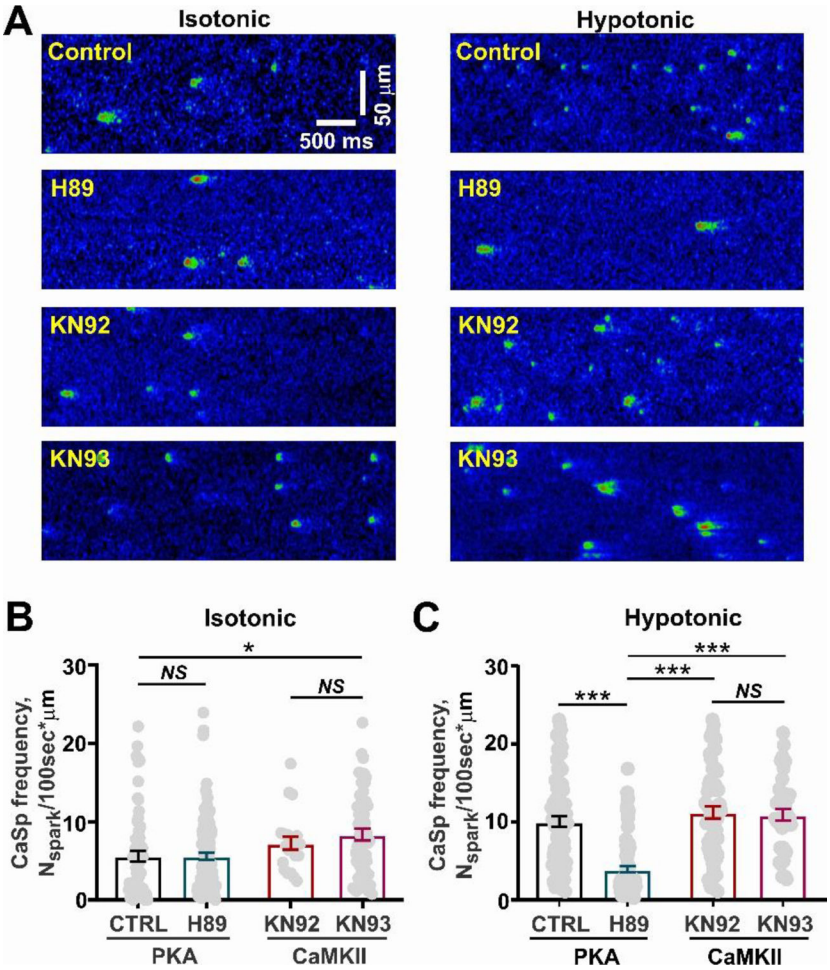

Fig. 7. PKA-mediated CaSp activity in swelled cells.

(A) Confocal line scans of Ca^{2+} spark activity in IT (*left*) and HT (*right*) treated ACM under control condition (without drugs) and after application of 1μM of H-89, 1μM of KN92, and 1μM of KN92. (B-C) Summarized data for the effects of PKA (H89) and CaMKII (KN93) inhibition on CaSp frequency in IT (B) and in HT (C) cells. IT: CTRL (n=31), H89 (n=56), KN92 (n=59), KN93 (n=54); HT: CTRL (n=60), H89 (n=64), KN92 (n=54), KN93 (n=40). from N=5 mice. *,*** – $p<0.05$, 0.001 by two-way ANOVA.

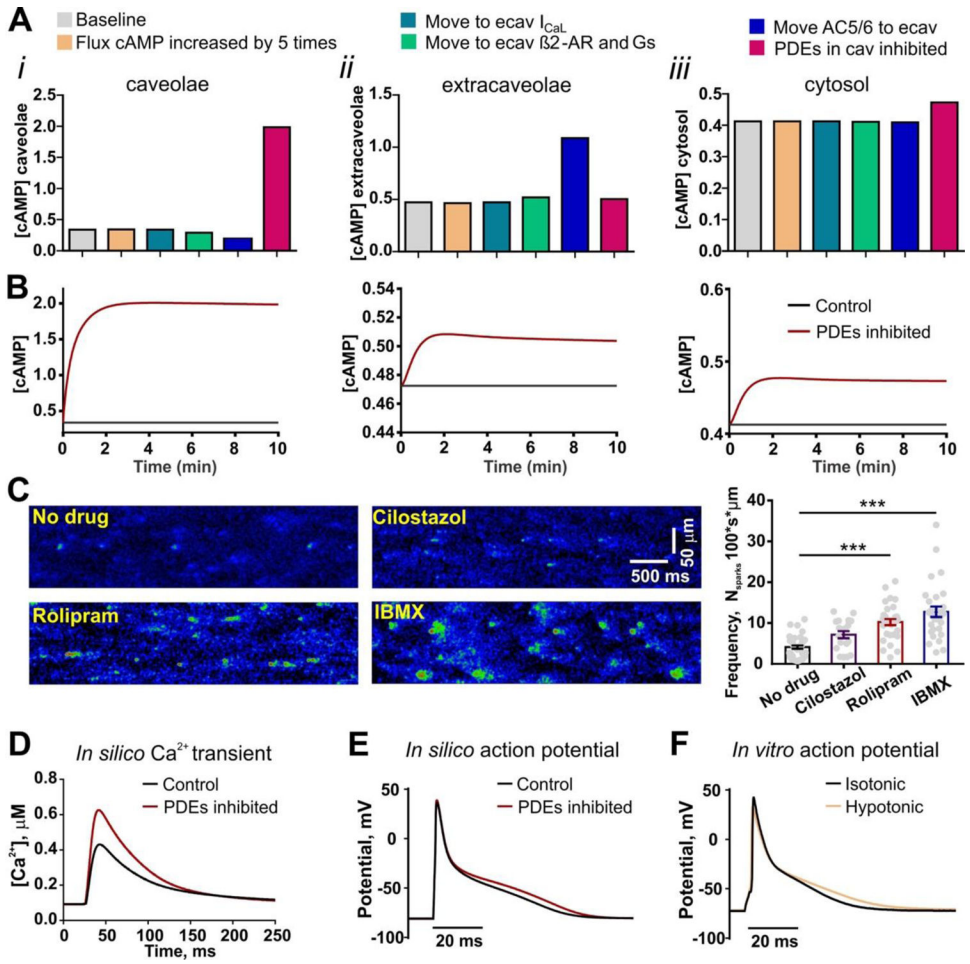

Fig. 8. Caveolae-specific PDE inhibition leads to cAMP upregulation, Ca^{2+} signaling augmentation and action potential prolongation.

(A) Mathematical modeling of the effects of caveolar protein changes on cAMP levels in caveolae (*i*), extracaveolae (*ii*) and cytosol (*iii*) compartments of ACM. (B) Simulation of microdomain-specific time courses of cAMP levels in ACM under baseline and under caveolae-specific PDE inhibition. (C) Typical Ca^{2+} spark confocal recordings (*left*) and statistical analysis of Ca^{2+} spark frequency (*right*) in ACMs without PDE inhibitors (n=40 cells) and after cilostazol (PDE3 inhibitor, n=19), rolipram (PDE4 inhibitor, n=32) and IBMX (non-selective PDE inhibitor, n=29) in isotonic condition. *** – $p<0.001$ by one-way ANOVA. (D-E) *In silico* simulation of Ca^{2+} transient (D) and AP (E) changes under caveolae-specific PDE inhibition. (F) *In vitro* mouse action potential under isotonic and hypotonic (2 min) conditions.